Journal of Inorganic and Organometallic Polymers and Materials (2025) 35:3014–3030
https://doi.org/10.1007/s10904-024-03440-6

RESEARCH

Facile Preparation of Cross-Linked *Moringa oleifera* Seed Hulls Powder/Hydroxyapatite Framework Composite for Efficient Removal of Toluidine Blue and Methyl Violet 2B from Aqueous Solution

Albert Mandjewil[1] · Patrick T. Ngueagni[2,3,4] · Patrick N. Fotsing[1] · Julien Vieillard[5] · Ngoungoure M. Fadimatou[1] · Opeyemi A. Oyewo[6] · Seshibe S. Makgato[6] · Damian C. Onwudiwe[2,4] · Ashmore Mawire[3] · Emmanuel D. Woumfo[1]

Received: 5 September 2024 / Accepted: 2 October 2024 / Published online: 23 October 2024

Abstract

In this study, adsorption of two cationic dyes, Toluidine Blue (TB) and Methyl violet 2B (MV 2B) from an aqueous solution was achieved by using multifunctional composite material. The formulation of the composite (MO@HA) was obtained by using *Moringa oleifera* seed hull powder, calcium chloride ($CaCl_2$), and ammonium hydrogenophosphate $(NH_4)_2HPO_4$ salts. Surface morphology, functional groups, specific surface area, and surface charge of the composite were explored using Scanning electron microscopy (SEM), Fourier Transform infrared spectroscopy (FTIR), BET analysis, and point of zero charge (PZC), respectively. The composite material resulted in a structural change in the surface of the adsorbents, increased oxygen vacancies, enhancement of active sites, and a specific surface area of 735.55 $m^2\ g^{-1}$. Different adsorption parameters such as pH, contact time, adsorbent dosage, and initial concentration were evaluated. The adsorption study showed that equilibrium was reached after 60 min, and the optimum adsorption pH for both dyes (TB and MV 2B) was 6. Langmuir, Freundlich, Liu, and Temkin were fitted to describe the adsorption isotherm, both TB and MV 2B had best correlation with Liu isotherm. The maximum adsorption capacity of TB and MV 2B were 341.488 and 182.453 mg g^{-1}, respectively. Adsorption-desorption cycling studies on the adsorbent confirmed its regeneration and reusability after 5 cycles. A possible adsorption mechanism involving electrostatic interactions, n-π bonding, and hydrogen bonding was suggested. These findings highlight a new direction in the development of efficient and sustainable adsorbent in environmental remediation, specifically in the removal of dyes from aqueous solution.

Keywords Composite Material · Toluidine Blue · Methyl Violet 2B · Isotherms · Adsorption Mechanism

✉ Patrick T. Ngueagni
nguetsop.ricks@gmail.com

✉ Emmanuel D. Woumfo
edjoufac2000@yahoo.fr

[1] Department of Inorganic Chemistry, Faculty of Science, University of Yaounde I, P.O Box 812, Yaounde, Cameroon

[2] Materials Science Innovation and Modelling (MaSIM) Research Focus Area, Faculty of Natural and Agricultural Science, North-West University (Mafikeng Campus), Mmabatho, South Africa

[3] Material Science, Innovation and Modelling (MaSIM) Research Focus Area, Department of Physics, North-West University, Mmabatho 2745, Mahikeng, South Africa

[4] Department of Chemistry, Faculty of Natural and Agricultural, Science, North-West University (Mafikeng Campus), Private Bag X2046, Mmabatho 2735, South Africa

[5] Normandie Université, UNIROUEN, INSA Rouen, CNRS, COBRA (UMR 6014), Evreux 27000, France

[6] Department of Chemical Engineering, College of Science, Engineering and Technology, University of South Africa (UNISA), c/o Christian de Wet & Pioneer Avenue, Florida Campus 1710, Johannesburg, South Africa

1 Introduction

Water pollution represents a critical global challenge that threatens both aquatic environment and human health in significant ways. Due to the rapid evolution of human industrial activities such as textile, tanning, pharmaceuticals, and cosmetics, water pollution has resulted to the contamination of effluents with organic dyes [1, 2] In recent years, textile industry has emerged as one of the most significant sectors and a massive income for many countries in the world. It is estimated that 700.000 tons of dyes and pigments are annually consumed worldwide, and textile industries represent two-thirds of the consumption [3]. Unfortunately, because of their complex aromatic structure, dyes are highly stable in water and resistant to biodegradation which extends their detrimental effects in water bodies. Furthermore, most of dyes are carcinogenic, hazardous, lethal even at low concentrations due to their toxicity, and can be discharged into water and in the environment [1, 4, 5]. Methyl violet 2B is one of the most used cationic dye characterized by its intense violet colour in water that hinders the photosynthesis process, negatively affects living organisms, and a wide range of disorder in human beings [4, 6]. Toluidine Blue (TB), also known as Tolonium chloride is a basic thiazine metachromatic dye used in forensic examination, manufacturing of chemicals, and in the production of dyestuff. However, recent studies reported that either ingestion or direct contact with TB can severely affect human health [7]. Therefore, it is important to remove these contaminants to safeguard the environment and promote water reuse.

Several approaches such as adsorption [8–10], advanced oxidation process [11], filtration [12], coagulation and flocculation [13], electrochemical [14], photocatalysis [15–17] have been reported for the removal of organic dye in aqueous solution. However, compared to other approaches, adsorption process is more acceptable due to its benefits such as relatively low cost, simplicity, eco-friendliness, no harmful byproduct, low sludge production, high regeneration, and reuse performance. Different materials have been used as adsorbents, however, a critical factor considered in the choice of materials is sustainability and cost-effectiveness.

Biomaterials derived from agricultural waste have attracted attention as a new type of adsorbents, because of the rich presence of polysaccharides and proteins with various functional groups such as carboxyl, hydroxyl, and phosphates [18]. Consequently, Vallisneria Natans [19], cocoa shell [10], waste potato peels [20], Lychaete pellucida [21], ipomoea aquatica [22], banana peel [23], Biochar/Delonix regia seed gum/chitosan [24], *Moringa oleifera* seeds [25], and rice husk [26] are different agro-wastes and aquatic waste commonly used as adsorbents for dye removal from textile effluents. Adsorbents such as activated carbons [27], clay adsorbents [28], zeolites [29], macroporous chitosan microspheres [30], and composite-based metal oxide-based adsorbents [6] have also been used in the process of removing dyes from aqueous media.

Moringa oleifera (MO) also is a polyvalent growing tree that belongs to the family of Moringaceae, and consists of different fruits including seeds, seed husks, and pods [31]. MO tolerates semiarid conditions, and thus can easily be found in sub-Saharan African countries. MO seeds are well known for their benefits and have been used as a green, versatile, inexpensive and available adsorbent for water treatment [32]. Hydroxyapatite [$Ca_{10}(PO_4)_6(OH)_2$] (HA) is the main inorganic component of hard tissues in human body, which can also be synthesized with calcium and phosphate salts. Because of its distinctive properties such as non-toxicity, high surface area, chemical and thermal stability, biocompatibility, eco-friendliness, and particular crystal structure, HA has been used as a promising adsorbent for the removal of organic pollutants and various dyes in solution [33, 34]. However, HA nanoparticles are prone to form aggregates in aqueous solution which can significantly reduce its surface area and removal effectiveness. The design and choice of modification method play an important role in the physicochemical properties and adsorption capacity of a material [24]. To the best of our knowledge, there are no reports on the preparation of crosslinked *Moringa oleifera* seed hull powder with hydroxyapatite (MO@HA) as a potential adsorbent for the removal of Toluidine Blue (TB) and Methyl violet 2B (MV 2B) cationic dyes. Therefore, preparing a composite material may improve the adsorption properties that each component cannot achieve separately.

Consequently, the main objective of this study was to explore the potential of a composite of *Moringa oleifera* seed hull powder, calcium chloride ($CaCl_2$), and ammonium hydrogenophosphate $(NH_4)_2HPO_4$ salts as an adsorbent for addressing the challenges of environmental pollution by dyes such as TB and MV 2B. The composite material was characterized by FT-IR, SEM, BET analysis, and point of zero charge. The adsorption behaviour was investigated by important parameters such as contact time, pH, adsorbent dosage, temperature, and coexisting ions on the adsorption of TB and MV 2B were studied. The adsorption characteristics of MO@HA were explored, and the data obtained from the adsorption isotherms were fitted to different models to better understand the interaction of the adsorbent with the pollutants. Desorption/regeneration study was performed to determine the reusability of MO@HA adsorbent.

2 2. Materials and Methods

2.1 Chemicals

Calcium chloride ($CaCl_2$, 97%), ammonium hydrogen phosphate ($(NH_4)_2HPO_4$, 98%), hydrochloric acid (HCl, 37%), sodium hydroxide (NaOH, 98%), sodium nitrate ($NaNO_3$, 99%), toluidine blue (TB), and methyl violet 2B (MV 2B) (Fig. 1) were purchased from Sigma Aldrich (Germany) were used as supplied. All solutions were prepared without any purification.

2.2 Moringa Hulls Harvesting and Preparation

Moringa seed hulls were collected from Goldavi village, located in the Far North Region of Cameroon. The hulls were manually separated from the seeds and washed with distilled water several times to get rid of suspended materials or possible contaminants. The recovered cellulosic material was sun-dried for a week, and then dried in an oven at 100 °C for 24 h. Once dried, it was ground by mortar and pestle, sieved through a 160 µm stainless steel. The obtained powder was stored in a glass container and labelled MOB. Subsequently, this powder was treated with sodium hydroxide solution (NaOH, 1 mol L^{-1}) to delignify the material, increase the number of adsorbent binding sites, and allow the availability of adsorption sites [10]. Thereafter, 5 g MOB was introduced into a 200 mL conical flask containing 100 mL sodium hydroxide (NaOH, 1 M) at 323 K and stirred continuously at 150 rpm for 90 min. After pretreatment, the mixture was filtered with Whatman filter paper, washed several times with distilled water until neutral pH was reached, and dried in an oven at 70 °C for 24 h. The resulting material was labelled MOA.

2.3 Preparation of Composite

The composite material was prepared as follows: 0.11 g of $CaCl_2$ (0.01 M) was dissolved in a 150 mL beaker containing 200 mL of distilled water and stirred vigorously for 10 min to completely dissolve the calcium chloride salt. To this solution, 4 g of MOA was added to form a suspension of a mixture designated as α. In another beaker containing 200 mL of distilled water, 0.66 g of $(NH_4)_2HPO_4$ (0.025 M) was dissolved and stirred until the ammonium hydrogen phosphate salt was completely dissolved (about 10 min), and the mixture formed was designated as β. The solutions α and β were then adjusted to a pH = 10.0 using solutions of HCl (0.1 M) and NaOH (0.1 M). Finally, solution β was added in dropwise to solution α while stirring continuosly. After 36 h of incubation, the precipitate formed was isolated and then washed four times with ethanol (98%) to remove the water and effectively isolate the precipitate. The resulting precipitate was oven-dried at 90 °C for 24 h to obtain the composite material labeled MO@HA, and kept in a tight container for further studies.

2.4 Characterization of Materials

The samples MOB, MOA, and MO@HA were characterized by using different techniques such as scanning electron microscopy (SEM), Fourier transform infrared spectroscopy (FTIR), BET analysis, and point of zero charge (pHpzc). For the SEM analysis, the adsorbents were gold plated at 18 mA for 360 s using a Biorad E5200, and images were acquired using a ZEISS EVO 15-electron microscope. Fourier transform infrared (FTIR) spectroscopy analysis was performed using a Tensor 27 spectrometer (Bruker) with a ZnSe ATR crystal with a scanning range from 4000 to 500 cm^{-1}. For

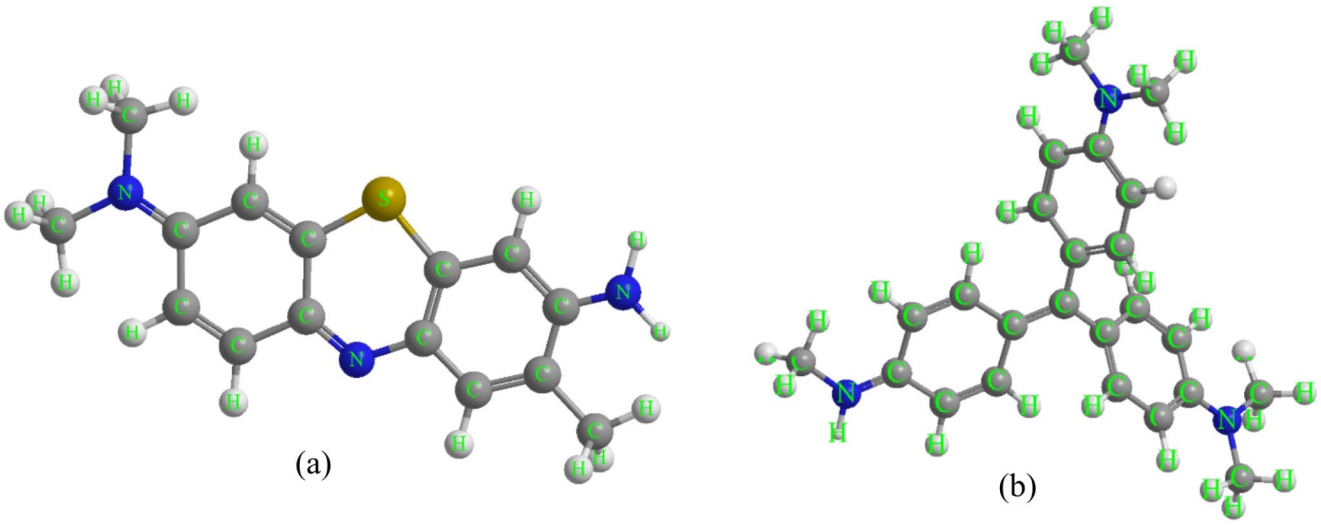

Fig. 1 Chemical structures of **a** TB and **b** MV 2B

each spectrum, 20 scans were recorded with a resolution of 4 cm^{-1}. The evaluation of specific surface area with BET analysis was achieved using Micrometrics Tristar II 3000 (USA). The solid addition method determined the pH values at the point of zero charge (pHpzc) of MOB, MOA, and MO@HA [8]. The pH values were determined using a Consort C 863 multiparameter electronic analyzer. The initial pH value (pH_i) of 50 mL of $NaNO_3$ (0.1 mol L^{-1}) solution was adjusted to the pH range of 2 to 12 using 0.1 mol L^{-1} of NaOH and HCl. Then, 0.1 g of each sample was introduced in a 100 mL conical flask containing 50 mL of $NaNO_3$ solution, then homogeniously stirred for 3 h and stored for 48 h to reach equilibrium at room temperature. The final pH (pH_f) of the solution was recorded, and pHpzc was found at $\Delta pH = 0$ from a plot of (pH_f - pH_i) versus pH_i.

2.5 Batch Adsorption and Desorption Studies

Numerous adsorption parameters for the removal of TB and MV 2B were investigated, including initial (pHi), adsorbent dosage (m), initial dye concentration (C_0), contact time (t), and temperature (T). For each adsorption experiment, in a 100 mL beaker containing a mass of 0.1 g of MO@HA, 50 mL of dye solutions were introduced with a concentration ranging from 50 to 300 mg L^{-1} and pHi ranging from 2 to 12. The mixture was then stirred at a constant speed of 200 rpm until reaching equilibrium (three equal measurements of the dye concentration in the liquid phase). The solutions were then analyzed colorimetrically using HACH DR 3900 spectrophotometer at maximum absorbance wavelength of 630 nm and 585 nm for TB and MV 2B, respectively. All the experiments were performed in triplicate and the average are presented in this study.

The effect of pHi on dye removal was carried out over a pH ranging from 2 to 12, and the adjustment of pHi was done by adding an aqueous solution of NaOH or HCl (0.1 mol L^{-1}). The optimal adsorbent mass was obtained by varying the amount of MO@HA (0.1–0.5 g) in 50 mL of the dye solutions until equilibrium was reached. The evaluation of the temperature effect was performed using five beakers of 100 mL, each containing 50 mL of a 100 mg L^{-1} Toluidine blue or Methyl violet 2B solution and 0.1 g of MO@HA stirred at different temperatures, including 293 K, 303 K, 313 K, 323 K and 333 K and pHi of 6 for TB and MV 2B, respectively.

The adsorption kinetics was studied using (0.1 g) adsorbent in 50 mL dye solutions at the initial pH with an initial dye concentration of 100 mg L^{-1} in 100 mL beakers. The suspensions were stirred at intervals ranging from 0 to 120 min to reach equilibrium. After a given time, the solution was filtered and then quantitatively analyzed.

Equilibrium adsorption isotherms were performed to determine the maximum adsorption capacity (q_{max}) at room temperature. For this purpose, 0.1 g of MO@HA was mixed with 50 mL of solutions with different initial pollutant concentrations ranging from 0 to 300 mg L^{-1} at initial pH. Then, the suspensions were stirred for a given equilibrium time.

The adsorption quantities at equilibrium (q_e in mg g^{-1}) were calculated using Eq. (1), and the percentage of adsorption (%R) was estimated using Eq. (2):

$$q_e = \frac{(C_0 - C_e)V}{m} \quad (1)$$

$$\%R = \frac{(C_0 - C_e)}{C_0} 100 \quad (2)$$

where C_0 and C_e are the initial and equilibrium concentrations (mg L^{-1}), respectively, V is the volume of the solution (L), and m is the mass of adsorbent used in (g).

The desorption experiments were performed using HCl solution (1×10^{-3} mol L^{-1}) as an eluent to estimate the reversibility of MO@HA and the recovery of Toluidine blue or Methyl violet 2B. The adsorbents were first equilibrated with the dyes in an aqueous solution with an initial concentration of 100 mg L^{-1}. Then the desorption test was initiated by mixing in the presence of HCl solution until the equilibrium time. After the desorption test, the adsorbents were thoroughly washed with distilled water and reused in the next round of adsorption experiments. The desorption and regeneration experiments were performed at room temperature. The amounts of dyes desorbed (q_{des}) and the efficiency (% des) were determined by Eqs. 3 and 4, respectively:

$$q_{des} = \frac{C_{des} V}{m} \quad (3)$$

$$\%_{des} = \frac{(C_f - C_r)}{C_f} 100 \quad (4)$$

where C_{des} is the concentration of dyes desorbed (in mg L^{-1}), V is the volume of the solution (in L), m is the mass of adsorbent (in g), C_f is the initial concentration of MO@HA loaded dye (in mg L^{-1}), and C_r is the final concentration of MO@HA loaded with dye (in mg L^{-1}).

The effect of coexisting ions consisted of evaluating the impact of chemical species such as NaCl and $CaCl_2$ in a range of concentration of 0.01 to 0.1 mg L^{-1} of dye concentration. The experiment was carried out at room temperature at 200 rpm with 0.1 g of MO@HA at maximum pH solution. The residual solutions were filtered and the solutions were then analyzed with the HACH DR 3900 spectrophotometer.

The respective adsorption quantities and removal percentages were obtained from Eqs. 1 and 2.

2.6 2.6 Mathematical Approaches for TB and MV 2B Adsorption onto MO@HA

Adsorption isotherms are essential for maximizing the practical use of adsorbents and explaining their interaction with adsorbates. In this study, adsorption isotherm was performed at room temperature, and the experimental data were simulated by three well-known isotherms including Langmuir, Freundlich, and Liu. The following relationships describe the non-linear form of these isotherms:

$$q_e = \frac{Q_{max}.K_L.C_e}{1 + K_L.C_e} \quad (5)$$

$$q_e = K_F.C_e^{1/nF} \quad (6)$$

$$q_e = \frac{Q_{max}.(K_g.C_e)^{nL}}{1 + (K_g.C_e)^{nL}} \quad (7)$$

$$q_e = \frac{RT}{b_T}.\ln(A_T C_e) \quad (8)$$

where q_e is the adsorbate amount adsorbed at equilibrium (mg g^{-1}); C_e is the adsorbate concentration at equilibrium (mg L^{-1}); Q_{max} is the maximum sorption capacity of the adsorbent (mg g^{-1}); K_L is the Langmuir equilibrium constant (L mg^{-1}); K_F is the Freundlich equilibrium constant [$mg.g^{-1}.(mg.L^{-1})^{-1/nF}$]; K_g is the Liu equilibrium constant (L mg^{-1}); n_F and n_L are the exponents of Freundlich and Liu model, respectively, (n_F and n_L are dimensionless), A_T is the Temkin isotherm (L g^{-1}), b_T is the constant related to the heat of adsorption (J mol^{-1}), T is the absolute temperature (K), and R is the universal gas constant (J mol^{-1} K^{-1}).

3 Results and Discussion

3.1 Characterization Results

3.1.1 FT-IR Spectral Analysis

The FT-IR spectra of MOB, MOA, and MO@HA are shown in Fig. 2, which display broad bands around 3373, 3374, and 3371 cm^{-1}, respectively. These bands are characteristic of the hydroxyl group (-OH) of either carboxylic acids, alcohols, and/or phenolic groups. The peaks located around 2931 and 2847 cm^{-1} are associated with -C-H and -CH2-groups, respectively [35]. These groups could be linked to the structure of the cellulose, hemicellulose, and lignin contained in the powdered hulls of the moringa seeds. The peaks around 2338 and 2366 cm^{-1}, which are present only in the spectrum of the MOA, could be attributed to the stretching vibrations of the O = C = O bonds. The bands that appeared around 1592, 1624, and 1627 cm^{-1} (between 1500 and 2000 cm^{-1}) are ascribed to the C-O stretching vibrations and N-H in-plane bending vibrations. These bands are characteristic of the primary and secondary amide structures [36]. The vibrational band due to the -C = C- group of aromatic compounds appeared around 1423 cm^{-1}, while the 1263 and 1265 cm^{-1} bands present in all three spectra may be attributed to the C-O vibration of the ester. The more intense band at 1033 cm^{-1} in the spectrum of MOA is the shifting of the-C-O bond to a lower frequency. This shift is confirmatory of the presence of phenolic compounds and carboxylic acids and also shows the lignocellulosic structure of the biosorbent [25]. These variations in the functional groups present in the biomaterial relates to the differences in the structure of lignin, hemicellulose, and cellulose in the hulls of moringa seeds. The more intense peak at around 1027 cm^{-1} in the spectrum of MO@HA composite material is due to the asymmetric stretching vibration of PO_4^3. The peak at 963 cm^{-1} is due to the bending vibration of the P-O-bond and was observed in the spectrum of the composite material (MO@HA), but was initially absent in the spectra of the pristine material (MOB) and the NaOH-activated material (MOA). The peak located at around 873 cm^{-1} in the spectrum of the MO@HA material is assigned to out-of-plane deformation vibrations of the C-H bonds of the aromatic compounds.

3.1.2 Scanning Electron Microscope (SEM)

Scanning Electron Microscopy was used to assess the morphological structure of unmodified and modified cellulose fibers obtained from Moringa seed hull powder. The micrographs obtained are shown in Fig. 3a-c. The image of MOB (Fig. 3(a)) reveals a structure with a leaf-like arrangement, less dense attributed to the irregularly shaped of lignocellulosic fibers. Likewise, the presence of white patches in the unmodified *Moringa oleifera* powder confirms the presence of hemicellulose. On the other hand, MOA (Fig. 3(b)) shows agglomerated and more densely fibrous structure which may be due to the pectin, cellulose, hemicellulose, lignin, and waxes emerging from the partial dissolution of polysaccharides components after sodium hydroxide treatment. The SEM image of MO@HA (Fig. 3(c)) shows a rough and cracked morphology with pores distributed across a compacted surface which is possibly attributed to the compositing of the MOA with HA layer, and this confirms a good adhesion of MOA with HA. The SEM microgram of this

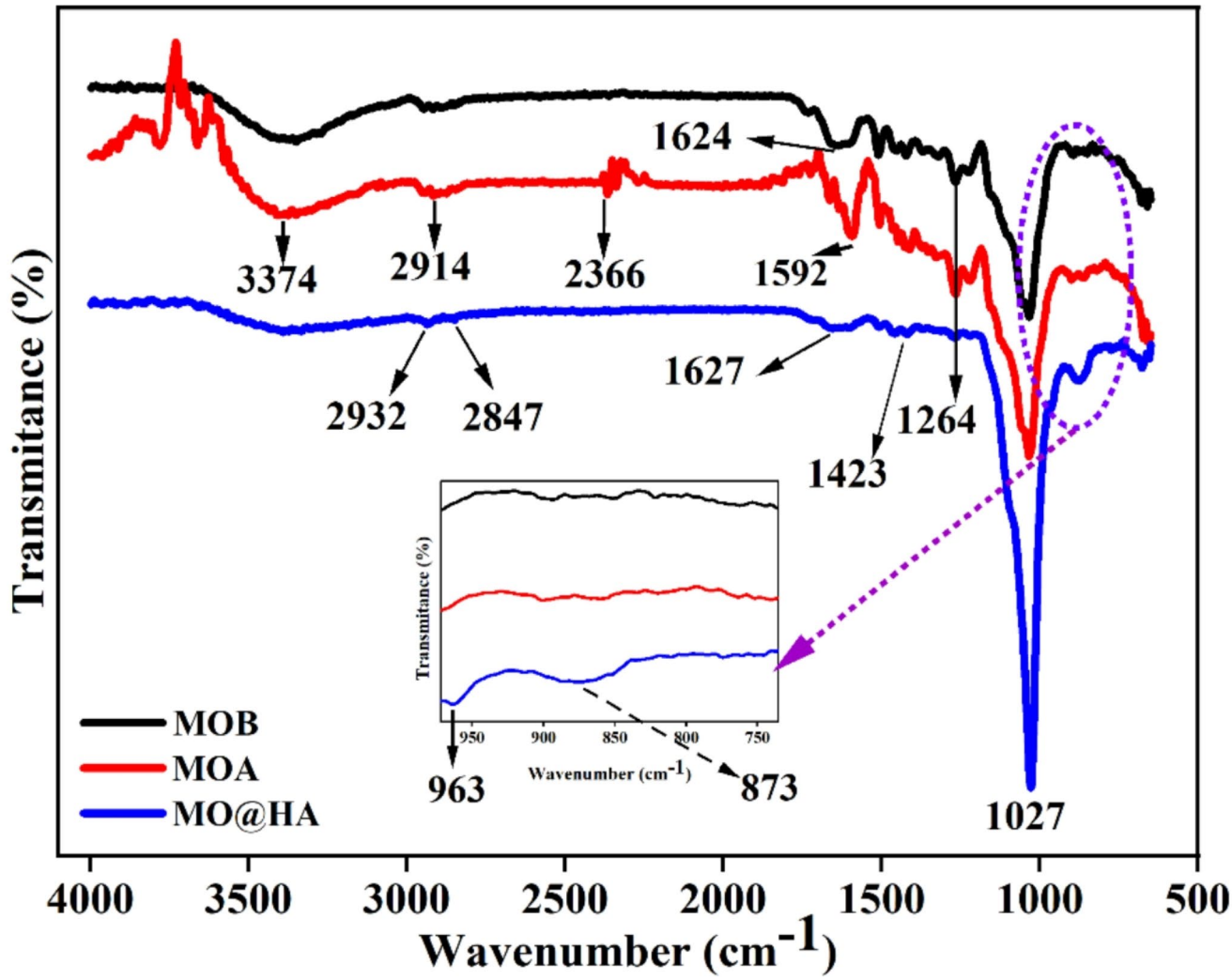

Fig. 2 FT-IR spectra of MOB, MOA, and MO@HA

composite reveals some interesting features regarding the texture and morphology of the material. Also, the composite material possesses pores, which increase the possibility for the absorption and trapping of dye molecules on the surface of the composite.

3.1.3 Brunauer Emmett Teller Surface Area

The results obtained from the N_2 equilibrium adsorption isotherms at 77 K are presented in Table 1. It was found that the surface area of crosslinked *Moringa oleifera* hull seed was evaluated to be 735.55 $m^2\ g^{-1}$. However, the values of unmodified (MOB) and treated *Moringa oleifera* with sodium hydroxide (MOA) were found to be 665.20 $m^2\ g^{-1}$ and 712.04 $m^2\ g^{-1}$, respectively. The increase of surface area is attributed to the presence of hydroxyapatite. The largest surface area suggests a good removal efficiency of dyes.

3.1.4 Point of Zero Charge (pHpzc)

The pH_{pzc} is the pH at which the net surface charge, resulting from the adsorption of the potential determining ions, H_3O^+ and OH^- is zero. At this value, the surface of the adsorbent is neutral ($pH = pH_{pzc}$), while it turns positively charged at lower pH values ($pH < pH_{pzc}$) or negatively charged at higher pH values ($pH > pH_{pzc}$) [37]. According to Fig. 4(a), the values of pH_{pzc} of MOB, MOA, and MO@HA are 3.5, 7.3, and 5.8, respectively. After basic activation of raw material (MOB) with NaOH, the pH_{pzc} increases from 3.5 (point of zero charge of raw material, MOB) to 7.3 (point of zero charge of activated material, MOA). The higher value of the alkali-activated material (MOA) is probably due to the presence of carboxylate and alcohol functions, provided by cellulose and NaOH base treatment. However, when the activated material is used to form a composite material with calcium chloride ($CaCl_2$) and diammonium hydrogen

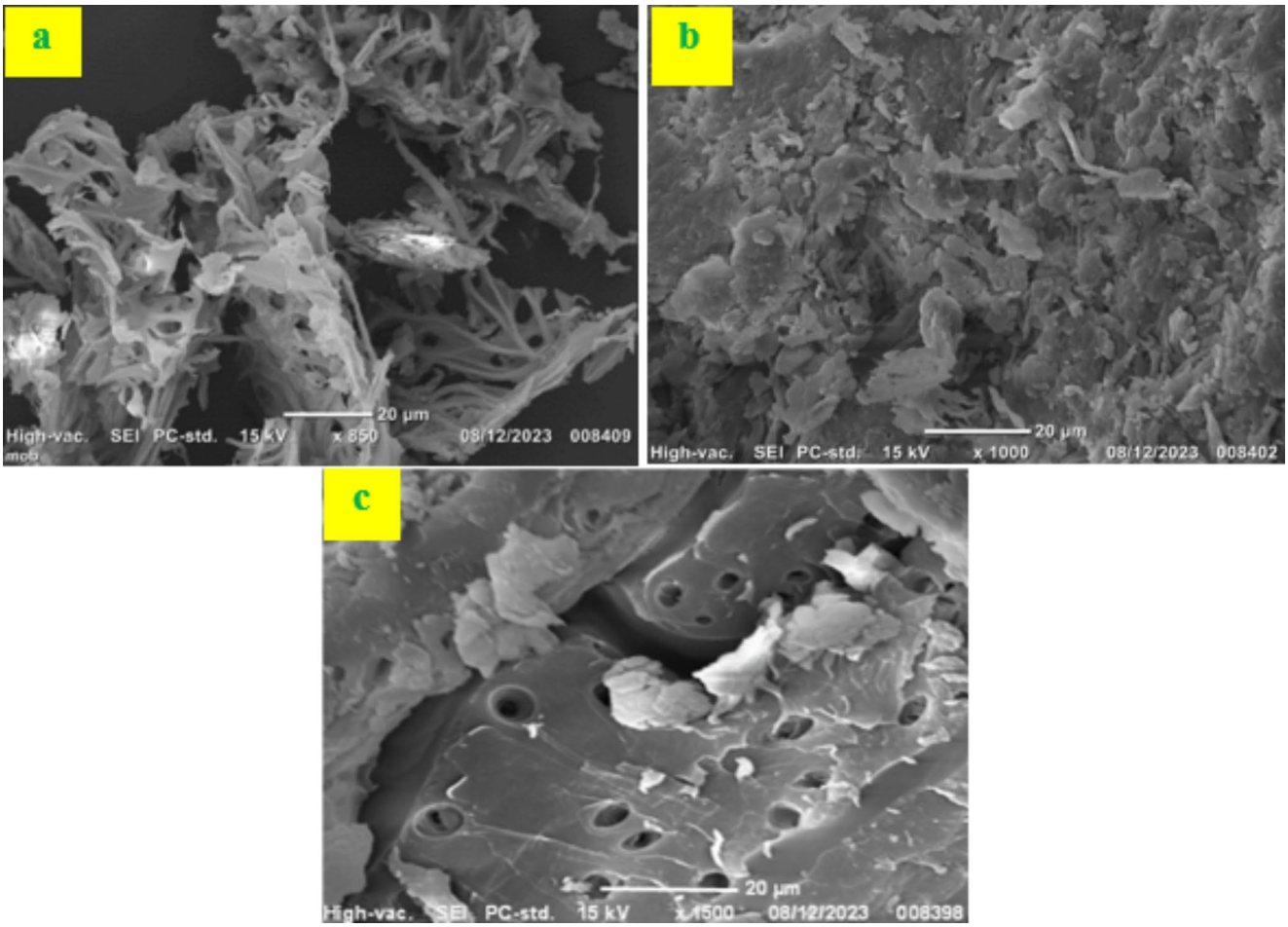

Fig. 3 SEM images of **a** MOB, **b** MOA, and **c** MO@HA

Table 1 BET analysis results of *Moringa oleifera* seed hulls powder/hydroxyapatite framework composite

Samples name	Single point surface area ($m^2\ g^{-1}$)	BET surface area ($m^2\ g^{-1}$)
MOB	664.0	665.20
MOA	710.0	712.04
MO@HA	734.3	735.55

phosphate salts, the pH_{pzc} decreases up to 5.8, probably caused by the acidic nature of calcium.

3.2 TB and MV 2B Adsorption Effectiveness onto Adsorbents

3.2.1 Study of Adsorbent Choice for TB and MV 2B dye Removal

Figure 4(b) shows a histogram of TB and MV 2B removal onto MOB, MOA, and MO@HA. This study demonstrates that natural MOB is relevant in capturing TB and MV 2B, but the performance of MO@HA is better with more than 140 mg g^{-1} of dye adsorbed. The poor dye adsorption observed for MOA could be attributed to the higher pHpzc of the MOA (7.3) than the pH (6.0) of the dye [38]. In this case (pHpzc > pH), repulsive interactions may occur between TB, MV 2B (cationic dyes), and the composite surface, since both dyes and the adsorbent surface have an overall positive charge. However, the composite MO@HA shows an increase in the adsorption capacities from 29.06 mg g^{-1} for MOA to 146.36 mg g^{-1} for MO@HA on TB dye adsorption. In the case of MV 2B, it shows an increase from 21.49 mg g^{-1} to 148.21 mg g^{-1}. The high adsorption capacity of MO@HA is due to the more negatively charged sites on the surface of the composite material, generated by the salt $(NH_4)_2HPO_4$, which promotes the adsorption of the TB and MV 2B cations [39]. Therefore, MO@HA was used as the main adsorbent material in this study.

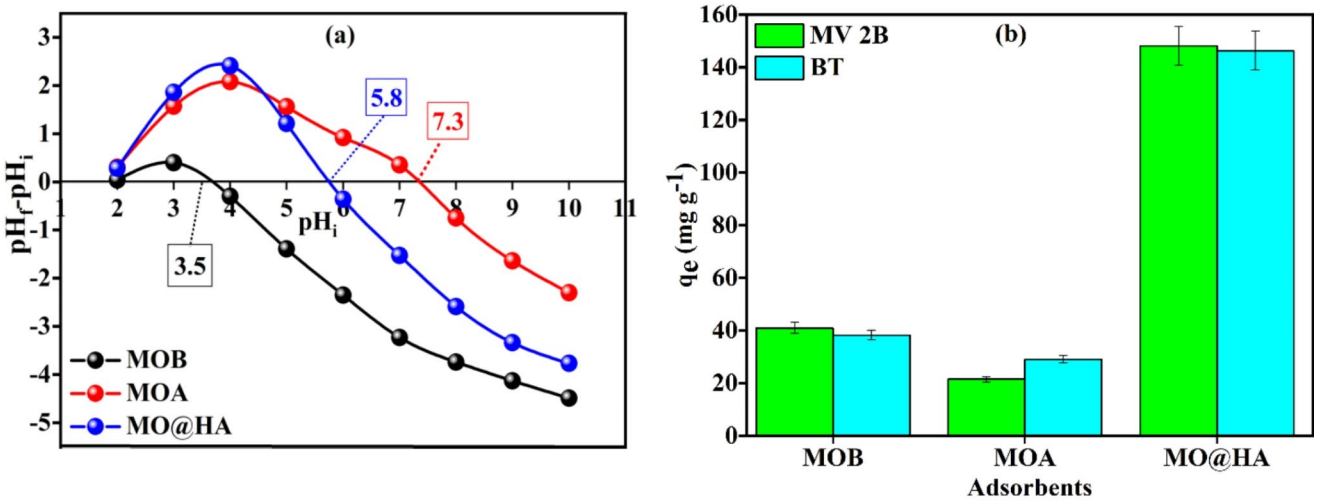

Fig. 4 **a** pH_{pzc} curves ($C_0 = 1$ mol L^{-1}; V = 50 mL; m = 0.1 g; Time = 2880 min; Room temperature); **b** adsorption capacities of MOB, MOA, and MO@HA ($C_0 = 50$ mg L^{-1}; V = 50 mL; m = 0.1 g; Time = 60 min; Room temperature)

3.2.2 Effect of pH

The pH is an important parameter in the dye sorption process. It controls the strength of electrostatic charges developed on the surface of the adsorbent during the dye adsorption [40]. The effect of pH on the adsorption of TB and MV 2B dyes onto MO@HA surfaces was studied within the initial pH range from 2 to 10. The experimental parameters such as contact time (1 h), dye concentration (100 mg L^{-1}), stirring speed (250 rpm), solution volume (50 mL), adsorbent dosage (0.1 g), and temperature (303 K) were kept constant. As shown in Fig. 5(a), the maximum adsorption quantities of 149.45 and 137.16 mg g^{-1} for TB and MV 2B respectively, take place at pH = 6 both for TB and MV 2B. In acidic conditions (pH around 6), the limited increase of adsorption capacities is due to the excess of H^+ ions that compete with the positive charge of dye solutions, resulting in an unfavorable optimum removal [38]. Moreover, at pH < pHzpc (5.8), repulsive interactions could have occurred between the cationic dyes (TB and MV 2B) molecules and the surface of the adsorbent since both of them had an overall positive charge. Furthermore, in acidic environments, the adsorption capacity could be impaired by the competition of H^+ ions with TB and MV 2B molecules [41]. At high pH (pH > pHzpc), the surface of composite MO@HA had more negatively charged sites, favoring the adsorption of TB and MV 2B on the sorbent [39]. It is therefore assumed that at pH > pHzpc the adsorption process takes place without significant loss of color of TB and MV 2B molecules. Here, pH = 6 was selected because it is close to the pH of natural water and industrial waste and it corresponds to the maximal adsorption capacity of MO@HA. Further batch adsorption studies for the reason that this pH value is higher than pHpzc (5.8) of the composite MO@HA affected to the satisfactory adsorption process via electrostatic interaction, and it is at this pH value that we obtain the maximum adsorption quantities for these two cationic dyes.

3.2.3 Effect of Adsorbent Dosage

The effect of the MO@HA (composite) dosage was studied to investigate the application of adsorbents on TB and MV 2B dye adsorption. The different adsorbent doses (0.1, 0.2, 0.3, 0.4, and, 0.5 g) were added into 50 mL of 100 mg L^{-1} TB and MV 2B dye solution. The solution was adjusted to the optimum pH of 6, obtained from the previous experience, at a temperature of 303 K, and a stirring speed of 250 rpm. Then, the adsorption was carried out for 1 h. The amount of composite material in the range of 0.1 to 0.5 g on TB and MV 2B adsorption was depicted in Fig. 5(b and c). As shown in these figures, the amount of TB and MV 2B adsorbed onto the MO@HA decreases respectively with increasing adsorbent dose. This may be due to many factors, one of them which is the increase in adsorbent dose leading to unsaturation of adsorption sites through the adsorption process. In the case of high adsorbent dosage, the agglomeration of biosorbent may occur in the solution and the biosorbent particles obstruct the interaction between dye molecules and active sites on the composite material surface [42, 43]. Agglomeration could lead to a decrease in the total surface area available on the adsorbent and an increase in diffusional path [44]. This situation could have negative effects on the adsorption process. As a result, the amount of composite material (MO@HA) at 0.1 g exhibited high adsorption performance of TB and MV 2B dye removal. From an economic point of view, this adsorbent dose is appropriate for further batch experiments.

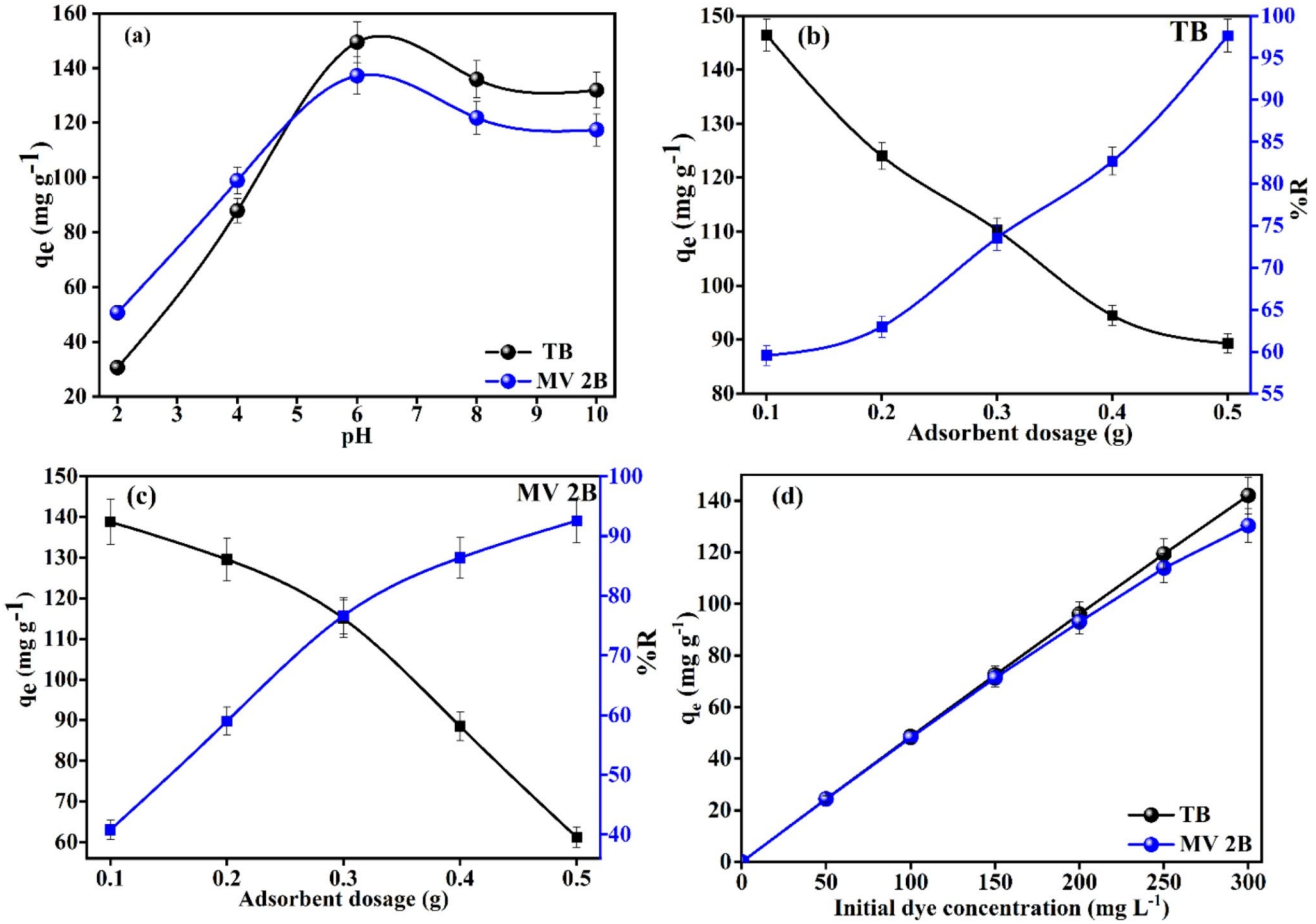

Fig. 5 **a** Effect of pH (C_0 = 100 mg L^{-1}; V = 50 mL; m = 0.1 g; Time = 60 min; Room temperature), **b** and **c** adsorbents dosage on the removal of TB and MV 2B (C_0 = 100 mg L^{-1}; V = 50 mL; Time = 60 min; pH = 6; Room temperature); **d** Initial concentration onto the prepared composite (V = 50 mL; m = 0.1 g; pH = 6; Time = 60 min; Room temperature)

3.2.4 Effect of Initial dye Concentration

Figure 5(d) shows the effect of initial concentration on the adsorption of TB and MV 2B at room temperature. It can be observed that the adsorption capacity (q_e) increases with increasing initial concentration indicating the higher affinity between TB and MV 2B with MO@HA. This is because, a higher adsorbate concentration in the solution increases the electrostatic repulsion between molecules present in the medium, thereby increasing the diffusion resistance for mass transfer inside the solution, but does not increase the diffusion resistance at the interface [45]. Generally, as the initial concentration of dye in a solution increases, the adsorption sites on the adsorbent surface become saturated, resulting in a decrease of removal efficiency. Also, increasing concentration leads to increase interaction between dye molecules and MO@HA material, thereby increasing the adsorption process.

3.2.5 Effect of Contact Time

The effect of contact time on dye removal by composite material was studied by variation of the contact time from 15 to 90 min. Figure 6 shows the adsorption capacity versus the adsorption time at various initial TB and MV 2B concentrations at room temperature. This figure shows that the amount of dye adsorbed on the MO@HA material increases with time and reaches equilibrium after 60 min. The removal of TB and MV 2B is faster in the first 15 min of the process probably due to the abundant availability of active sites on the MO@HA surface and rapid diffusion through the composite material pores by mass transfer. However, with the gradual occupancy of the sites, the sorption of TB and MV 2B becomes less efficient. Beyond 60 min, the kinetic adsorption is slower and the amount of adsorbed TB and MV 2B dyes did not significantly change with time, probably due to the saturation of adsorption sites of MO@HA. In view of all these, 60 min was taken as the equilibrium time in batch adsorption experiments.

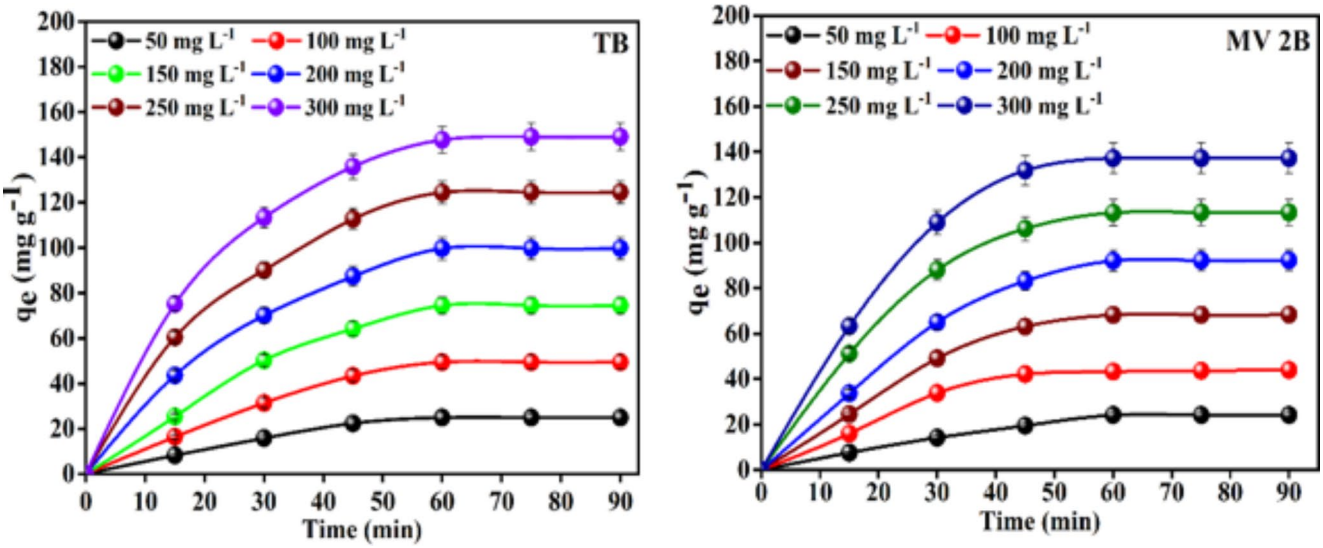

Fig. 6 Effect of contact time on the removal of TB and MV 2B (V = 50 mL; m = 0.1 g; pH = 6; Room temperature)

Table 2 Adsorption parameters of isotherm models

	TB	MV 2B
Langmuir		
Q_{max} (mg g^{-1})	252.2143	157.7071
K_L (L mg^{-1})	0.0796	0.1135
R^2_{adj}	0.9987	0.9969
SD (mg g^{-1})	1.8295	2.6461
Freundlich		
K_F (mg g^{-1} (mg $L^{-1})^{-1/nF}$)	25.3243	28.9395
n_F	1.5872	2.3624
R^2_{adj}	0.9968	0.9828
SD (mg g^{-1})	2.9172	6.2305
Liu		
Q_{max} (mg g^{-1})	341.4881	182.4533
K_g (L mg^{-1})	0.0424	0.0782
n_L	0.8593	0.8303
R^2_{adj}	0.9996	0.9990
SD (mg g^{-1})	0.9784	1.4875
Temkin		
K_{Te} (L mg^{-1})	1.1694	1.3647
b_{Te} (J mol^{-1})	54.6000	76.7000
R^2_{adj}	0.9567	0.9886
SD (mg g^{-1})	0.9912	0.9977

Table 3 Comparison of MO@HA adsorbent performance with other adsorbentsfor the removal of TB and MV 2B

Adsorbents	Q_{max} (mg g^{-1})	pH	References
TB dyes			
Orange peel waste	313.40	6.0	[50]
Giombo persimmon seed	34.73	8.0	[51]
Macroporous chitosan microspheres	187.69	6.0	[30]
karaya gum	149.64	7.0	[52]
MO@HA	341.49	6.0	Present work
MV 2B dyes			
Modified mangosteen pericarp	47.75	6.0	[53]
Activated carbon of oak with ZnO and Fe_2O_3	48. 59	9.0	[6]
Modified carobs	62.50	9.0	[54]
Cross-Linked Chitosan-Genipin/ Algae	71.90	8.4	[2]
Glutaraldehyde Crosslinked Chitosan-Algae-Montmorillonite	98.30	8.3	[4]
Chitosan-grafted salicylaldehyde/ algae	115.60	8.04	[55]
Food-grade algae modified Schiff base-chitosan	126.51	8.68	[56]
Coal-Based Activated Carbon	134.10	9.12	[57]
Treated Okoume sawdust	102.00	9.0	[58]
MO@HA	182.45	6.0	Present work

3.3 Adsorption Isotherms

The adsorption isothermal equilibrium study was conducted by fitting the experimental data with the Langmuir, Liu, Freundlich, and Temkin models. Equilibrium experimental curves were obtained under the following conditions: temperature (298 K), pH (6), contact time (60 min), adsorbent dosage 0.1 g, and initial TB, MV 2B dye concentration between 50 and 300 mg L^{-1}.

As shown in Table 2, the correlation coefficients (R^2_{adj}) of the nonlinear form for Liu's model of TB and MV 2B dyes are 0.9996 and 0.9909 respectively, and the low standard deviation (SD) values of TB and MV 2B are 0.9784 and 1.4875 respectively, indicating that, the Liu model isotherm is consistent for the two dyes. The equilibrium data for TB and MV 2B adsorption on the MO@HA adsorbents are well correlated. The maximum adsorption capacities (q_{max}), shown by Liu's model are 341.49 and 182.45 mg g^{-1} for TB and MV 2B, respectively. This model predicts that

the active sites of adsorbents cannot have the same energy [46].

The separation factor (R_L) value obtained from the Langmuir isotherm model decreased with increasing the initial dyes concentration and it lies in the range ($0 < R_L < 1$) suggesting the suitability of the prepared adsorbents for the adsorption process of TB and MV 2B dyes from aqueous solutions [47].

The value of n determines the affinity of the process, chemisorption ($n_F < 1$), or physical adsorption ($n_F > 1$). From Fig. 7(c), the Freundlich plot gives a n_F value of 1.587 and 2.362 for TB and MV 2B dyes respectively, indicating that physical adsorption occurs [48]. Generally, physical adsorption is driven by the presence of van der Waals bonds between the adsorbate and adsorbent. The difference between these two values is (0.775), and this low variation demonstrated the heterogeneous surfaces of MO@HA composite material and the high favourability of TB and MV 2B adsorption onto the prepared adsorbent [47].

The adsorption energy terms b_{Te} for TB and MV 2B determined according to the Temkin model were 76.7 and 54.6 J mol^{-1}, respectively. These energy values are positive, indicating that the adsorption reaction is exothermic [49].

Analysis of Table 3 reveals that the MO@HA composite material developed in this work presents a better performance on TB and MV 2B removal compared to the different adsorbent materials listed.

3.4 3.4. Effect of Co-existing Ions

One of the elements that regulates the electrostatic and non-electrostatic interactions between the adsorbate and the adsorbent surface is the solution's ionic strength [59]. Apart from dyes, wastewater from the textile and dye-producing sectors contains a variety of suspended and dissolved chemicals that might be regarded as contaminants in the dye-removal process. Usually, the most prevalent metal ions found in wastewater containing dyes are cations, such as Na^+, K^+, Ca^{2+}, Cr^{3+}, and Cu^{2+} [60]. High ionic strength, which is caused by the presence of ions, can have a major impact on how well the biosorption process works. In this study, the effects of ionic strength and co-existing ions on the adsorption quantity of TB and MV 2B dye using MO@HA composite were investigated using NaCl and $CaCl_2$ solutions at concentrations ranging from 0 to 0.1 mol L^{-1}. As depicted in Fig. 8, the effect of ionic strength examined in this study showed a decreasing trend in removal capacity with increasing salt concentration in the solution. The outcomes demonstrated that the elimination of TB and MV 2B dye was less effective in the presence of Na^+ and Ca^{2+} ions in aqueous solutions. The hydrated ion radius may be the cause of this decline in decontamination of efficiency because smaller ions may compete with larger dye molecules for space on the adsorbent's surface, decreasing the effectiveness of the adsorption process [61]. Furthermore, it should be mentioned that Ca^{2+} has a greater capacity than Na^+ to decrease the TB and MV 2B dye adsorption efficiency. The ionic radius, molecular weight, and electric charges of Ca^{2+} ions may be the fundamental causes [6].

3.5 3.5. Desorption and Reusability

In order to recover the dye adsorbed on the MO@HA surface and regenerate the adsorbent for future use, 10^{-2} mol L^{-1} of HCl solution was used as the eluent to protonate the acid sites of MO@HA and remove the dyes. As can be seen in Fig. 9, the amount of desorbed pollutants decreases with time. This is explained by the fact that pollutants are released from the material as the desorption time increases. In both cases, the desorption quantities of 1.190 mg g^{-1} of TB and 1.508 mg g^{-1} of MV 2B were reached at 480 min. The very low dye desorption indicates that the dye molecules are bound through strong interaction [10, 62].

In order to avoid the useless economic cost of the adsorption process, the reuse of adsorbents is a great importance. Following the TB and MV 2B dye adsorption process onto the composite material (MO@HA), 50 mL of HCl solution (1×10^{-2} mol L^{-1}) was added to the adsorbents for 1 h to perform chemical regeneration. The results showed that after five cycles, the adsorption efficiency decreased slightly (Fig. 10).

This decrease could also be due to the degradation of the adsorbent during the process on one hand, and the loss of small quantities of the adsorbent during the filtration on the other hand. The MO@HA composite performed well in removing TB and MV 2B from the aqueous solution, based on the results.

3.6 3.6 Adsorption Mechanism

Cross-linking Moringa olëifera seed hull powder with $CaCl_2$ and $(NH_4)_2HPO_4$ is a chemical process designed to improve the powder's properties and make it more effective for various applications. The cross-linking mechanism steps can be explained as follows: *Moringa oleifera* seed hull powder contains functional groups such as hydroxyls, carboxyls and amines. Thus, the $CaCl_2$ reacts with the hydroxyl groups in the powder to form calcium bonds, and then $(NH_4)_2HPO_4$ reacts with carboxyl groups in the powder to form phosphate bonds. The calcium and phosphate bonds create a three-dimensional network that links the powder particles together. The FTIR spectra displayed an abundance of functional groups such as hydroxyl and phosphate groups available at the surface of composite material which drive

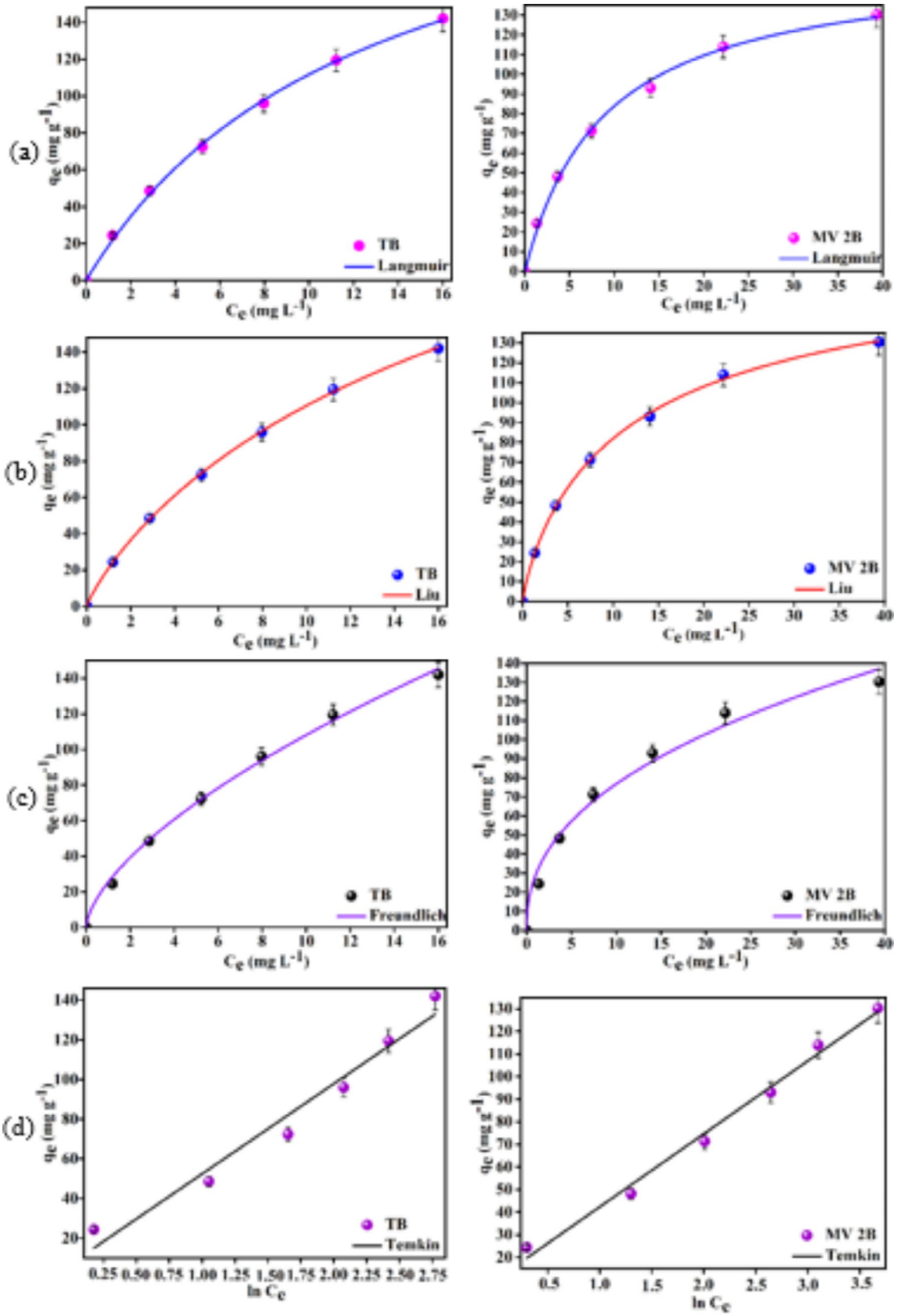

Fig. 7 Isotherms curves of TB and MV 2B adsorption by MO@HA (V = 50 mL; m = 0.1 g; Time = 60 min; pH = 6 ; Room temperature)

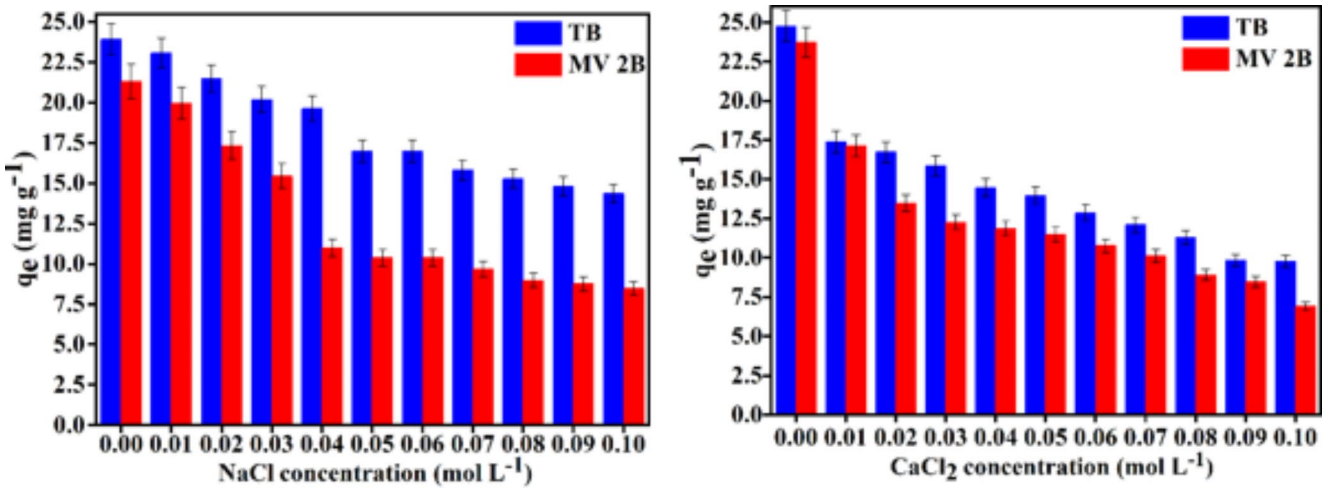

Fig. 8 Effect of ionic strength on the adsorption of TB and MV 2B dye uptake (V = 50 mL; m = 0.1 g; Time = 60 min; pH = 6; Room temperature)

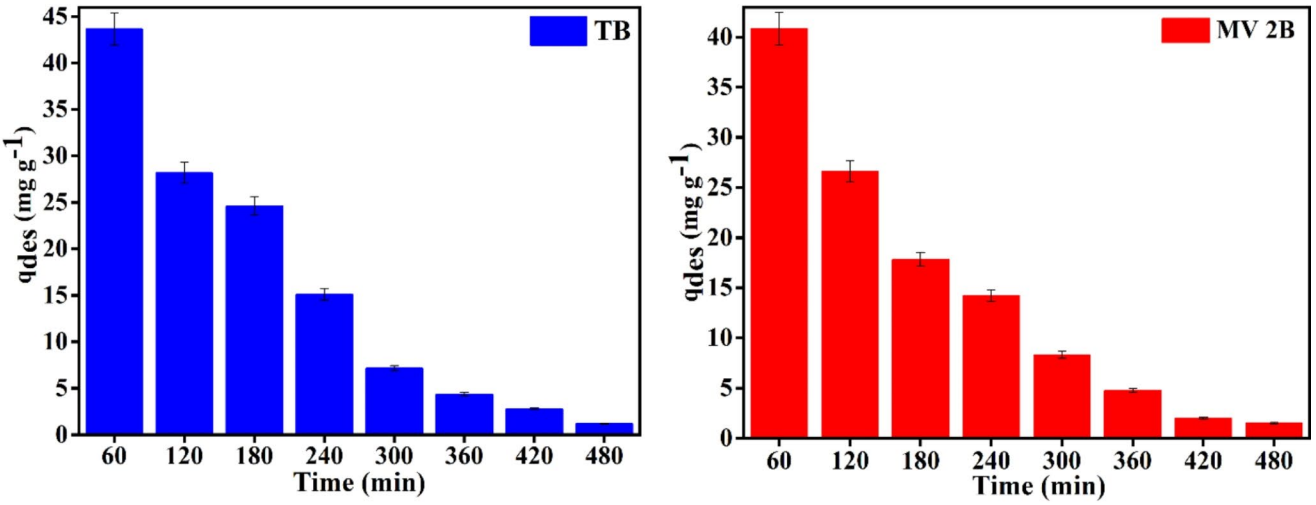

Fig. 9 Desorption of TB and MV 2B from MO@HA (C_0 = 100 mg L^{-1} ; V = 50 mL; m = 0.1 g; pH = 6; Room temperature)

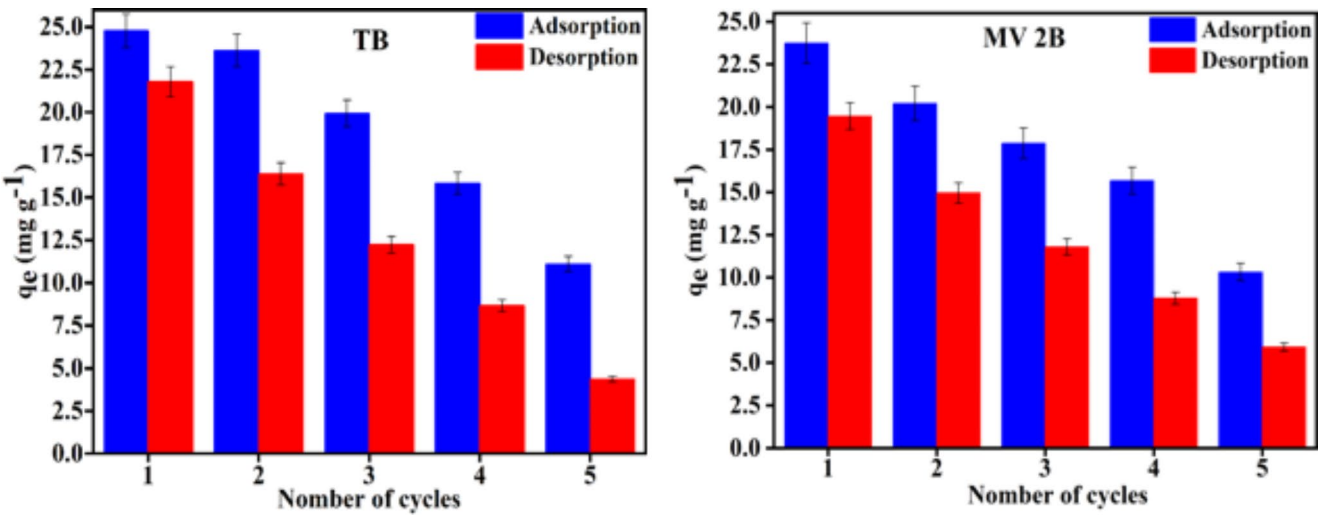

Fig. 10 Effect of reuse on the performance of MO@HA in removing BT and MV 2B dyes from aqueous solution (C_0 = 100 mg L^{-1}; V = 50 mL; m = 0.1 g; pH = 6, Time = 60 min; Room temperature)

the adsorption process. The interactions between functional groups and the dye molecules are represented in Fig. In an aqueous medium where pH > pHpzc, the functional groups are negatively charged, therefore a strong electrostatic attraction is established with the positively charged MV 2B molecules, contributing to the adsorption process as shown in Fig. 11. Moreover, the hydrogen bonds interactions play an important role in the adsorption process. Nitrogen heteroatoms of MV 2B dye molecules interact with hydrogen atoms on the surface of MO@HA to generate hydrogen bonds. Finally, the interaction between oxygen groups on the composite material and the arene rings of MV 2B generate n-π interactions that enhance the overall adsorption capacity.

In the case of Toluidine Blue dye, hydrogen-binding interactions may take place between hydrogen atoms of MO@HA and heteroatom (N and S) at the surface of the TB dye molecule. Moreover, the positive and negatively charged species of TB and MO@HA might also be involved during the adsorption process. The n-π interaction may occur between heteroatom-containing the composite material and aromatic rings of TB.

4 4 Conclusion

The effective removal of dyes toluidine blue (TB) and methyl violet 2B (MV 2B) using an MO@HA composite is a new process used that is reported in this work. According to the characterization analyses, the prepared composite material exhibited characteristics such as porosity, functional groups, and surface charge which can optimize the adsorption capacity of cationic dyes. Batch method experiments were realized at room temperature to study the effect of different parameters on the adsorption of TB and MV 2B onto MO@HA material. The results showed that the optimal pH of the adsorption medium for both dyes (TB and MV 2B) is 6 with a maximum adsorbent dosage of 0.1 g for an equilibrium time of 60 min. The maximum adsorption capacity (q_{max}) obtained for TB and MV 2B were 341.488 and 182.453 mg g^{-1}, respectively. The study of the effect of coexisting ions showed that Ca^{2+} has a greater capacity than Na^{+} to decrease the adsorption efficiency of TB and MV2B dyes on MO@HA material when in the same medium. It was shown that the sorbents can be regenerated in solutions of acids of which HCl is the most effective. The dye adsorption-desorption cycle study on the MO@HA material was performed efficiently for five (05) cycles. The prepared composite material proved to be an economical, renewable, and high-performance adsorbent.

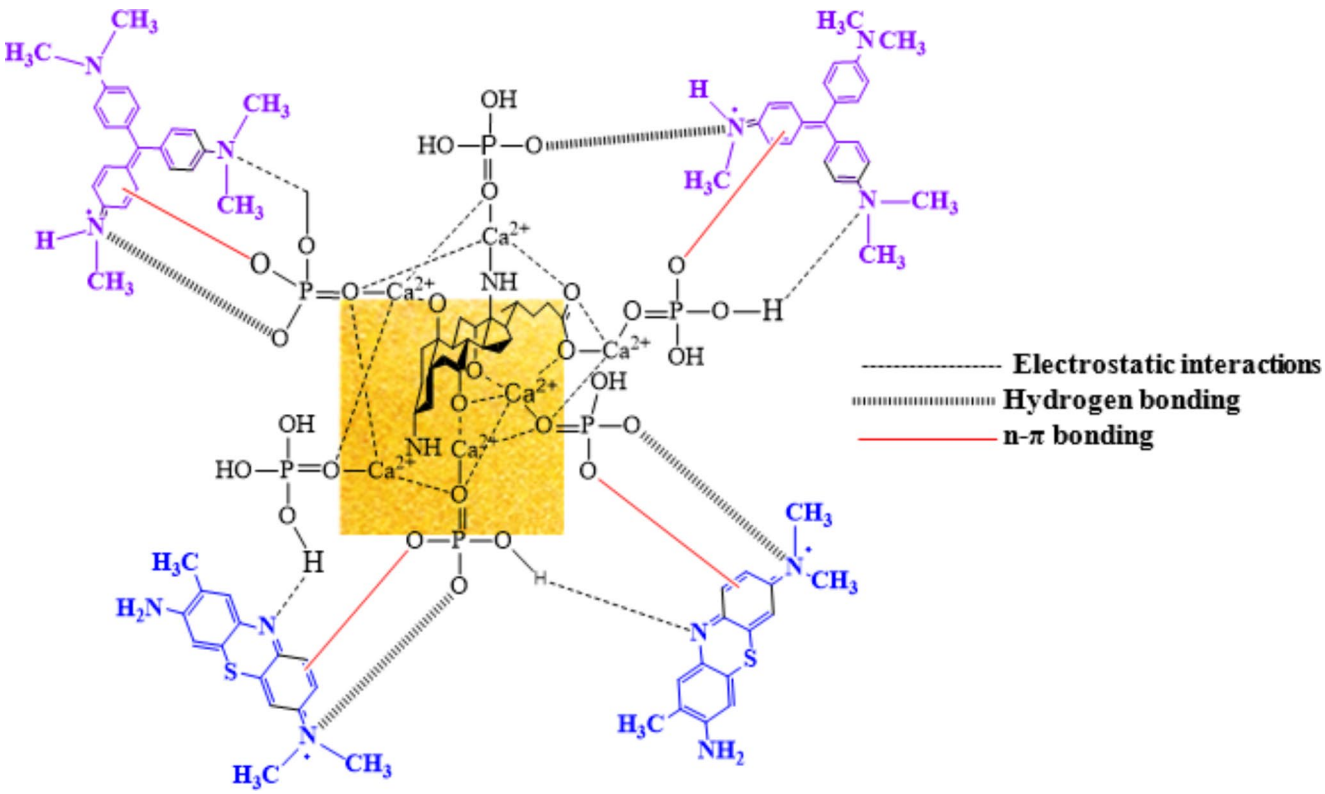

Fig. 11 Suggested adsorption mechanism for the removal of TB and MV 2B by MO@HA

Acknowledgements Acknowledgment to Materials Science Innovation and Modelling (MaSIM) Research Focus Area, Faculty of Natural and Agricultural Science, North-West University (Mafikeng Campus), Mmabatho, South Africa.

Author Contributions Albert Mandjewil: Writing-first draft, editing, methodology software. Patrick Tsopbou Ngueagni: Conceptualization, methodology, writing-original draft, editing. Patrick Fotsing Nkuigue: Writing-review, methodology, editing, software. Julien Vieillard: Material analysis, writing review, editing; Ngoungoure Mandou Fadimatou: Editing, methodology software; Opeyemi A. Oyewo: Validation, writing-review, editing, software; Seshibe Makgato: Validation, editing, software; Damian Chinedu Onwudiwe: Material analysis, writing review, editing; Ashmore Mawire: Writing-review, editing, Emmanuel Djoufac Woumfo: Supervision, validation, writing-review, editing.

Funding Open access funding provided by North-West University.

Data Availability The datasets used and/or analyzed during the current study are available from the corresponding author on reasonable request.

Declarations

Competing Interests The authors declare no competing interests.

References

1. K.M. Rehan, K.A. Basha, S.M. Safiullah, Synthesis of poly(Glycidyl Methacrylate) based hybrid materials and evaluation of methylene blue adsorption: structural characterization and adsorption behaviour. J. Inorg. Organomet. Polym. Mater. **33**(7), 2172–2187 (2023). https://doi.org/10.1007/s10904-023-02671-3
2. H.M. Agha, A.S. Abdulhameed, A.H. Jawad, T. Khadiran, Z.A. ALOthman, L.D. Wilson, Facile synthesis of cross-linked Chitosan-Genipin/algae composite adsorbent for cationic methyl violet dye removal: robust modeling of adsorption using the box–Behnken design. J. Inorg. Organomet. Polym. Mater. (2024). https://doi.org/10.1007/s10904-024-03327-6
3. E. Rápó, S. Tonk, Factors affecting synthetic dye adsorption; Desorption studies: a review of results from the last five years (2017–2021). Molecules **26**(17), 5419 (2021). https://doi.org/10.3390/molecules26175419
4. M.S. Sando, A.M. Farhan, A.H. Jawad, Schiff-base system of glutaraldehyde crosslinked chitosan-algae-montmorillonite Clay K10 biocomposite: adsorption mechanism and optimized removal for methyl Violet 2B Dye. J. Inorg. Organomet. Polym. Mater. (2024). https://doi.org/10.1007/s10904-024-03295-x
5. V. Jegatheesan, B.K. Pramanik, J. Chen, D. Navaratna, C.Y. Chang, L. Shu, Treatment of textile wastewater with membrane bioreactor: a critical review. Bioresour. Technol. **204**, 202–212 (2016). https://doi.org/10.1016/J.BIORTECH.2016.01.006
6. R. Foroutan, R. Mohammadi, A. Ahmadi, G. Bikhabar, F. Babaei, B. Ramavandi, Impact of ZnO and Fe3O4 magnetic nanoscale on the methyl violet 2B removal efficiency of the activated carbon oak wood. Chemosphere **286**, 131632 (2022). https://doi.org/10.1016/J.CHEMOSPHERE.2021.131632
7. R.L. Harris, F.A. Patty, *Patty's Industrial Hygiene* (Wiley, New York, 2000)
8. P.N. Fotsing et al., Removal of Cu(II) from aqueous solution using a composite made from cocoa cortex and sodium alginate. Environ. Sci. Poll. Res. **27**(8), 8451–8466 (2020). https://doi.org/10.1007/s11356-019-07206-3
9. P.T. Ngueagni, P.S. Kumar, E.D. Woumfo, S.M. Prasanth, Adsorption of Pb(II) and Cd(II) ions onto modified biogenic slaughterhouse waste: equilibrium and kinetic analysis. Int. J. Environ. Anal. Chem. **102**(16), 4344–4363 (2022). https://doi.org/10.1080/03067319.2020.1784409
10. A. Mandjewil et al., Correlation between cocoa shell modifications by CTAB and its dye adsorption properties. Environ. Sci. Pollut. Res. **30**(41), 94474–94484 (2023). https://doi.org/10.1007/s11356-023-28671-x
11. L. Liu et al., Treatment of industrial dye wastewater and pharmaceutical residue wastewater by advanced oxidation processes and its combination with nanocatalysts: a review. J. Water Process. Eng. **42**, 102122 (2021). https://doi.org/10.1016/J.JWPE.2021.102122
12. I. Ćurić, D. Dolar, J. Bošnjak, Reuse of textile wastewater for dyeing cotton knitted fabric with hybrid treatment: Coagulation/sand filtration/UF/NF-RO. J. Environ. Manag. **295**, 113133 (2021). https://doi.org/10.1016/J.JENVMAN.2021.113133
13. C. Zhao et al., Application of coagulation/flocculation in oily wastewater treatment: a review. Sci. Total Environ. **765**, 142795 (2021). https://doi.org/10.1016/j.scitotenv.2020.142795
14. J. Ding et al., Synergetic adsorption and electrochemical classified recycling of cr(VI) and dyes in synthetic dyeing wastewater. Chem. Eng. J. **384**, 123232 (2020). https://doi.org/10.1016/J.CEJ.2019.123232
15. D. Kanakaraju, M.H. bin Ya, Y.C. Lim, A. Pace, Combined Adsorption/Photocatalytic dye removal by copper-titania-fly ash composite. Surf. Interfaces. **19**, 100534 (2020). https://doi.org/10.1016/J.SURFIN.2020.100534
16. J. Leichtweis, S. Silvestri, E. Carissimi, New composite of pecan nutshells biochar-ZnO for sequential removal of acid red 97 by adsorption and photocatalysis. Biomass Bioenergy. **140**, 105648 (2020). https://doi.org/10.1016/J.BIOMBIOE.2020.105648
17. T.O. Ajiboye, O.A. Oyewo, D.C. Onwudiwe, Simultaneous removal of organics and heavy metals from industrial wastewater: a review. Chemosphere **262**, 128379 (2021). https://doi.org/10.1016/j.chemosphere.2020.128379
18. K.S. Bharathi, S.T. Ramesh, Removal of dyes using agricultural waste as low-cost adsorbents: a review. Appl. Water Sci. **3**(4), 773–790 (2013). https://doi.org/10.1007/s13201-013-0117-y
19. M. Abu Musa, S. Chowdhury, S. Biswas, S.M. Nur Alam, S. Parvin, M. Abdus Sattar, Removal of aqueous methylene blue dye over Vallisneria Natans biosorbent using artificial neural network and statistical response surface methodology analysis. J. Mol. Liq. **393**, 123624 (2024). https://doi.org/10.1016/J.MOLLIQ.2023.123624
20. K. Bouhadjra, W. Lemlikchi, A. Ferhati, S. Mignard, Enhancing removal efficiency of anionic dye (Cibacron blue) using waste potato peels powder. Sci Rep **11**(1), 2090 (2021). https://doi.org/10.1038/s41598-020-79069-5

21. H.A. Khalaf, M.M. El-Sheekh, M.E.M. Makhlof, Lychaete Pellucida as a novel biosorbent for the biodegradation of hazardous azo dyes. Environ. Monit. Assess. **195**(8), 929 (2023). https://doi.org/10.1007/s10661-023-11518-w
22. T.L. Kua, M.R.R. Kooh, M.K. Dahri, N.A.H.M. Zaidi, Y. Lu, L.B.L. Lim, Aquatic plant, Ipomoea aquatica, as a potential low-cost adsorbent for the effective removal of toxic methyl violet 2B dye. Appl. Water Sci. **10**(12), 243 (2020). https://doi.org/10.1007/s13201-020-01326-9
23. V.S. Munagapati, V. Yarramuthi, Y. Kim, K.M. Lee, D.S. Kim, Removal of anionic dyes (Reactive Black 5 and Congo Red) from aqueous solutions using Banana Peel Powder as an adsorbent. Ecotoxicol. Environ. Saf. **148**, 601–607 (2018). https://doi.org/10.1016/J.ECOENV.2017.10.075
24. A.F. Hassan, N.S. Awwad, H.A. Ibrahium, A.F. El-Kott, Biochar/Delonix regia seed gum/chitosan composite as efficient adsorbent for the elimination of phenol from aqueous medium. Int. J. Biol. Macromol. **273**, 132771 (2024). https://doi.org/10.1016/j.ijbiomac.2024.132771
25. Y. Raji, A. Nadi, I. Mechnou, M. Saadouni, O. Cherkaoui, S. Zyade, High adsorption capacities of crystal violet dye by low-cost activated carbon prepared from Moroccan *Moringa oleifera* wastes: characterization, adsorption and mechanism study. Diam. Relat. Mater. **135**, 109834 (2023). https://doi.org/10.1016/j.diamond.2023.109834
26. S. Chakraborty, S. Chowdhury, P. Das Saha, Adsorption of crystal violet from aqueous solution onto NaOH-modified rice husk. Carbohydr. Polym. **86**(4), 1533–1541 (2011). https://doi.org/10.1016/j.carbpol.2011.06.058
27. M. Sultana, M.H. Rownok, M. Sabrin, M.H. Rahaman, S.M.N. Alam, A review on experimental chemically modified activated carbon to enhance dye and heavy metals adsorption. Clean. Eng. Technol. **6**, 100382 (2022). https://doi.org/10.1016/j.clet.2021.100382
28. A. Rahman, T. Urabe, N. Kishimoto, Color removal of reactive Procion dyes by Clay Adsorbents. Procedia Environ. Sci. **17**, 270–278 (2013). https://doi.org/10.1016/J.PROENV.2013.02.038
29. I. Humelnicu, A. Băiceanu, M.E. Ignat, V. Dulman, The removal of Basic Blue 41 textile dye from aqueous solution by adsorption onto natural zeolitic tuff: kinetics and thermodynamics. Process Saf. Environ. Prot. **105**, 274–287 (2017). https://doi.org/10.1016/J.PSEP.2016.11.016
30. L. Qiao, K. Du, Toluidine blue-immobilized macroporous chitosan microspheres for highly efficient purification of fucoidan. Biochem. Eng. J. **108176**, 206 (2021). https://doi.org/10.1016/J.BEJ.2021.108206
31. V.U. Nwagbara, K. Chigayo, W.A. Iyama, H.M. Kwaambwa, Removal of lead, cadmium, and copper from water using *Moringa oleifera* seed biomass. J. Water Climate Change **13**(7), 2747–2760 (2022). https://doi.org/10.2166/wcc.2022.091
32. L.A. Araujo et al., *Moringa oleifera* biomass residue for the removal of pharmaceuticals from water. J. Environ. Chem. Eng. **6**(6), 7192–7199 (2018). https://doi.org/10.1016/j.jece.2018.11.016
33. H. Bensalah, S.A. Younssi, M. Ouammou, A. Gurlo, M.F. Bekheet, Azo dye adsorption on an industrial waste-transformed hydroxyapatite adsorbent: kinetics, isotherms, mechanism and regeneration studies. J. Environ. Chem. Eng. (2020). https://doi.org/10.1016/j.jece.2020.103807
34. M.S. Kothari et al., Sustainable synthesis of carbide slag waste derived hydroxyapatite and its application for cationic dye adsorption. J. Water Process. Eng. (2024). https://doi.org/10.1016/j.jwpe.2024.106001
35. P. Garside, P. Wyeth, Identification of cellulosic fibres by FTIR spectroscopy - Thread and single fibre analysis by attenuated total reflectance. Stud. Conser. **48**(4), 269–275 (2003). https://doi.org/10.1179/sic.2003.48.4.269
36. I.A. Ahmed, H.S. Hussein, A.H. Ragab, N. AlMasoud, A.A. Ghfar, Investigation the effects of Green-synthesized copper nanoparticles on the performance of activated Carbon-Chitosan-Alginate for the removal of cr(VI) from aqueous solution. Molecules **26**(9), 2617 (2021). https://doi.org/10.3390/molecules26092617
37. A.E. Ofomaja, Y.S. Ho, Effect of temperatures and pH on methyl violet biosorption by Mansonia wood sawdust. Bioresour. Technol. **99**(13), 5411–5417 (2008). https://doi.org/10.1016/J.BIORTECH.2007.11.018
38. S.M. Musyoka, H. Mittal, S.B. Mishra, J.C. Ngila, Effect of functionalization on the adsorption capacity of cellulose for the removal of methyl violet. Int. J. Biol. Macromol. **65**, 389–397 (2014). https://doi.org/10.1016/J.IJBIOMAC.2014.01.051
39. I. Loulidi et al., Adsorption of crystal violet onto an agricultural waste residue: kinetics, isotherm, thermodynamics, and mechanism of adsorption. Sci. World J. **2020**, 1–9 (2020). https://doi.org/10.1155/2020/5873521
40. Y. Önal, C. Akmil-Başar, D. Eren, Ç. Sarici-Özdemir, T. Depci, Adsorption kinetics of malachite green onto activated carbon prepared from Tunçbilek lignite. J. Hazard Mater. **128**(2–3), 150–157 (2006). https://doi.org/10.1016/J.JHAZMAT.2005.07.055
41. X. Wang, Y. Zhang, R. Shan, H. Hu, Polydopamine interface encapsulating graphene and immobilizing ultra-small, active Fe3O4 nanoparticles for organic dye adsorption. Ceram Int. **47**(3), 3219–3231 (2021). https://doi.org/10.1016/J.CERAMINT.2020.09.160
42. M.R. Kulkarni, T. Revanth, A. Acharya, P. Bhat, Removal of Crystal Violet dye from aqueous solution using water hyacinth: Equilibrium, kinetics and thermodynamics study. Resour. Efficient Technol. **3**(1), 71–77 (2017). https://doi.org/10.1016/J.REFFIT.2017.01.009
43. R. Ben Arfi, S. Karoui, K. Mougin, A. Ghorbal, Adsorptive removal of cationic and anionic dyes from aqueous solution by utilizing almond shell as bioadsorbent. EuroMediterr J. Environ. Integr. **2**(1), 20 (2017). https://doi.org/10.1007/s41207-017-0032-y
44. N.A. Oladoja, A.K. Akinlabi, Congo red biosorption on palm kernel seed coat. Ind. Eng. Chem. Res. **48**(13), 6188–6196 (2009). https://doi.org/10.1021/ie801003v
45. B.H. Hameed, Equilibrium and kinetic studies of methyl violet sorption by agricultural waste. J. Hazard. Mater. **154**, 1–3 (2008). https://doi.org/10.1016/J.JHAZMAT.2007.10.010
46. Y. Liu, A general model for biosorption of Cd^{2+}, Cu^{2+} and Zn^{2+} by aerobic granules. J. Biotechnol. **102**(3), 233–239 (2003). https://doi.org/10.1016/S0168-1656(03)00030-0
47. T.E. Khalil, A.F. Elhusseiny, A. El-dissouky, N.M. Ibrahim, Functionalized chitosan nanocomposites for removal of toxic cr (VI) from aqueous solution. React. Funct. Polym. **146**, 104407 (2020). https://doi.org/10.1016/J.REACTFUNCTPOLYM.2019.104407
48. K. Anwar Mohamad, Said et al., Application of Freundlich and Temkin Isotherm to study the removal of Pb(II) Via Adsorption on activated Carbon equipped Polysulfone membrane. Int. J. Eng. Technol. 7, 91 (2018). https://doi.org/10.14419/ijet.v7i3.18.16683
49. A. Balouch, M. Kolachi, F.N. Talpur, H. Khan, M.I. Bhanger, Sorption kinetics, isotherm and thermodynamic modeling of defluoridation of ground water using natural adsorbents. Am. J. Analyt Chem. **04**(05), 221–228 (2013). https://doi.org/10.4236/ajac.2013.45028
50. R. Lafi, S. Rezma, A. Hafiane, Removal of toluidine blue from aqueous solution using orange peel waste (OPW). Desalination Water Treat **56**(10), 2754–2765 (2015). https://doi.org/10.1080/19443994.2014.982962

51. M.S. Bretanha, G.L. Dotto, J.C.P. Vaghetti, S.L.P. Dias, E.C. Lima, F.A. Pavan, Giombo persimmon seed (GPS) an alternative adsorbent for the removal Toluidine Blue dye from aqueous solutions. Desalination Water Treat **57**(58), 28474–28485 (2016). https://doi.org/10.1080/19443994.2016.1179223
52. B.K. Preetha, B. Vishalakshi, Microwave assisted synthesis of karaya gum based montmorillonite nanocomposite: characterisation, swelling and dye adsorption studies. Int. J. Biol. Macromol. **154**, 739–750 (2020). https://doi.org/10.1016/J.IJBIOMAC.2020.03.107
53. A.P.P.W.A.S.R. Suwattanamala, Modified mangosteen pericarp powder as a biosorbent for removal of methyl violet 2B from aqueous solutions
54. B.A.M.S. Kerzabi, Y., Removal of methyl violet 2B dye from aqueous solution by adsorption onto raw and modified carobs (Ceratonia siliqua L.), *Global NEST J.*, 2022, https://doi.org/10.30955/gnj.004347
55. H.M. Agha, A.S. Abdulhameed, R. Wu, A.H. Jawad, Z.A. ALOthman, S. Algburi, Chitosan-grafted salicylaldehyde/algae composite for methyl violet dye removal: adsorption modeling and optimization. Int. J. Phytoremed. **26**(8), 1348–1358 (2024). https://doi.org/10.1080/15226514.2024.2318777
56. H.M. Agha et al., Food-grade algae modified Schiff base-chitosan benzaldehyde composite for cationic methyl violet 2B dye removal: RSM statistical parametric optimization. Int. J. Phytorem. **26**(4), 459–471 (2024). https://doi.org/10.1080/15226514.2023.2246596
57. S.A. Musa, A.S. Abdulhameed, S.N.A. Baharin, Z.A. ALOthman, L.D. Wilson, A.H. Jawad, Coal-Based activated carbon via microwave-assisted ZnCl2 activation for methyl violet 2b dye removal: optimization, desirability function, and adsorption mechanism. Minerals **13**(3), 438 (2023). https://doi.org/10.3390/min13030438
58. E. Khamssa, G. Guechi, S. Benabdesselam, O. Hamdaoui, E.-K. Guechi, Biosorption of methyl violet 2B by chemically treated Okoume sawdust: Kinetic, Isotherm and Thermodynamic studies. [Online]. Available: https://www.researchgate.net/publication/368982455
59. C.E. de Farias Silva, A.H. da Silva, Gonçalves, A.K. de Souza Abud, Treatment of textile industry effluents using orange waste: a proposal to reduce color and chemical oxygen demand. Water Sci. Technol. **74**(4), 994–1004 (Aug. 2016). https://doi.org/10.2166/wst.2016.298
60. V.M. Correia, T. Stephenson, S.J. Judd, Characterisation of textile wastewaters - a review. Environ. Technol. **15**(10), 917–929 (1994). https://doi.org/10.1080/09593339409385500
61. T. Shahnaz, M. M. F. S., P. V.C., and, S. Narayanasamy, Surface modification of nanocellulose using polypyrrole for the adsorptive removal of Congo red dye and chromium in binary mixture. Int. J. Biol. Macromol. 151, 322–332 (2020). https://doi.org/10.1016/J.IJBIOMAC.2020.02.181
62. X. Chen et al., Adsorption of copper and zinc by biochars produced from pyrolysis of hardwood and corn straw in aqueous solution. Bioresour. Technol. **102**, 8877–8884 (2011). https://doi.org/10.1016/J.BIORTECH.2011.06.078